Blue-detuned evanescent field surface traps for neutral atoms based on mode interference in ultrathin optical fibres

You may also be interested in:

Nanostructured optical nanofibres for atom trapping
M Daly, V G Truong, C F Phelan et al.

Optical nanofibres and neutral atoms
Thomas Nieddu, Vandna Gokhroo and Síle Nic Chormaic

Two-colour atom guide and 1D optical lattice using evanescent fields of high-order transverse modes
Jian Fu, Xiang Yin and Limin Tong

Pumping of higher-order modes of an optical nanofiber by laser excited atoms
A V Masalov and V G Minogin

A state-insensitive, compensated nanofiber trap
C Lacroûte, K S Choi, A Goban et al.

Integrated optical dipole trap for cold neutral atoms with an optical waveguide coupler
J Lee, D H Park, S Mittal et al.

Hyperfine spectroscopy of optically trapped atoms
A Kaplan, M F Andersen, T Grünzweig et al.

Controlled insertion and retrieval of atoms coupled to a high-finesse optical resonator
M Khudaverdyan, W Alt, I Dotsenko et al.

The formation of Coulomb clusters in a magnetic trap
S F Savin, L G D'yachkov, M I Myasnikov et al.

Blue-detuned evanescent field surface traps for neutral atoms based on mode interference in ultrathin optical fibres

G Sagué, A Baade and A Rauschenbeutel[1]

Institut für Physik, Universität Mainz, 55128 Mainz, Germany
E-mail: arno.rauschenbeutel@uni-mainz.de

Abstract. We present and analyse a novel concept for blue-detuned evanescent field surface traps for cold neutral atoms based on two-mode interference in ultrathin optical fibres. When two or more transverse modes with the same frequency co-propagate in the fibre, their different phase velocities cause a stationary interference pattern to establish. Intensity minima of the evanescent field at any distance from the surface can be created and an array of optical microtraps can thus be obtained around the fibre. We discuss three possible combinations of the lowest order modes, yielding traps at 100–200 nm from the fibre surface which, using a few tens of milliwatts of trapping laser power, have a depth of the order of 1 mK for caesium atoms and a trapping lifetime exceeding 100 s. The resulting trapping geometry is of particular interest because atoms in such microtrap arrays will be coupled to any additional field propagating in the fibre via the evanescent field, thereby realizing ensembles of fibre-coupled atoms.

[1] Author to whom any correspondence should be addressed.

IOP Institute of Physics Φ DEUTSCHE PHYSIKALISCHE GESELLSCHAFT

Contents

1. Introduction

Recently, the production of ultrathin optical fibres with diameters smaller than the wavelength of the guided light has become possible in a number of laboratories [1]–[4]. Such fibres have attracted considerable interest in the field of quantum optics due to their high potential for efficiently coupling light and matter [3, 5, 6]. The guided modes in such ultrathin optical fibres exhibit a unique combination of strong transverse confinement and pronounced evanescent field [7]. Furthermore, the strong radial confinement is maintained over the full length of the fibre waist, exceeding the Rayleigh range of a comparably focused freely propagating Gaussian beam by several orders of magnitude. This has been used in a number of experiments to couple atoms and molecules to the fibre mode via the evanescent field, showing that tapered optical fibres (TOFs) are a powerful tool for their detection, investigation and manipulation. Recently, evanescent field spectroscopy of a very small number of cold caesium atoms around a 500 nm diameter TOF has been performed [6]. In a similar experiment, the fluorescence of resonantly irradiated atoms around a 400 nm diameter TOF, coupled into the fibre mode, has been detected and spectrally analysed [3, 8]. The absorbance of organic dye molecules, deposited on a subwavelength-diameter TOF, has also been spectroscopically characterized via the fibre transmission with unprecedented sensitivity [9]. Finally, it has also been proposed to trap and guide atoms above planar waveguides and around ultrathin fibres using the optical dipole force exerted by a two-colour evanescent field [10]–[12]. In this case, the atoms can be coupled to and trapped near a dielectric nanostructure without the need of additional external light fields.

Here, we present a novel type of blue-detuned evanescent field trap for cold neutral atoms based on two-mode interference in such ultrathin optical fibres. We consider a field–fibre configuration where only the four lowest order modes propagate, the fundamental mode, HE_{11}, and the first three higher order modes, TE_{01}, TM_{01} and HE_{21}. If the modes are coherently excited, they will yield a stationary interference pattern while co-propagating in the fibre due to their different phase velocities. Previously, a similar scheme has been proposed for trapping

atoms in the evanescent field of a two-dimensional planar waveguide. In this case, however, the interference of at least four waveguide modes is required in order to achieve three-dimensional confinement of the atoms [13].

We explore all possible pairs of modes that can be used to trap cold neutral atoms in the intensity minima formed at the positions of destructive interference in the evanescent field surrounding the fibre. These combinations are $HE_{11} + TE_{01}$, $HE_{11} + HE_{21}$ and $TE_{01} + HE_{21}$.[2] We assume a cylindrical ultrathin silica fibre with 400 nm radius for all three trapping configurations. The wavelength and the total power of the guided light as well as the power distribution between the modes have been chosen to fulfil the following criteria for each individual trapping configuration: a three-dimensional trapping potential for caesium atoms, a depth of the trap of the order of 1 mK, and a trapping lifetime exceeding 100 s for an atom with an initial kinetic energy corresponding to a temperature of 100 μK.

This paper is organized as follows: section 1 is devoted to the analysis of the modal dispersion in ultrathin optical fibres and to the presentation of the electric field equations in the evanescent field for the three considered modes. In section 2, the trap arising from the interference between the HE_{11} and the TE_{01} mode is presented ($HE_{11} + TE_{01}$). Sections 3 and 4 then treat the $HE_{11} + HE_{21}$ and $TE_{01} + HE_{21}$ traps, respectively.

2. Electric field and mode propagation in ultrathin optical fibres

2.1. Mode propagation

We consider a step-index optical fibre consisting of a cylindrical bulk of dielectric material with radius a and refractive index n_1, surrounded by a second dielectric medium with infinite radius and refractive index n_2. For the guided light in such a fibre, a discrete set of propagation modes exists whose axial propagation constant β is fixed by the boundary conditions [14]. The number of modes and their axial propagation constant is then determined by the radius of the fibre a, the refractive indices of the two media, n_1 and n_2, and the wavelength of the light λ via the parameter $V = (2\pi a/\lambda)\sqrt{n_1^2 - n_2^2}$.

Figure 1 shows the axial propagation constant β for the first seven modes in the fibre normalized to the wavenumber in free space k_0 as a function of the V parameter. Note that β/k_0 lies between n_2 and n_1 which is a condition that must be fulfilled by any lossless mode [14]. In the following, β will be referred to as propagation constant or phase velocity. The dashed vertical line located at $V = 3.11$ corresponds to the three configurations considered in this paper, i.e. an ultrathin optical fibre of pure silica ($n_1 = 1.452$) with a radius $a = 400$ nm, surrounded by vacuum ($n_2 = 1$), and three similar wavelengths $\lambda = 849.0$ nm, 850.5 nm and 851.0 nm. In this case, only four modes are allowed to propagate, the fundamental mode HE_{11} and the first three non-fundamental modes, i.e. TE_{01}, TM_{01} and HE_{21}. At this value of V the phase velocities of all modes differ significantly. This difference will cause an interference pattern to establish along the fibre and, in addition, results in different radial decay lengths of the evanescent field outside the fibre for each mode. The modal dispersion can therefore be used to create a tailored evanescent field resulting from the interference of two or more co-propagating modes.

---

[2] The TM_{01} mode cannot be used to create a trap because its polarization at the position of destructive interference cannot be matched with any of the other modes due to its large component in the direction of propagation.
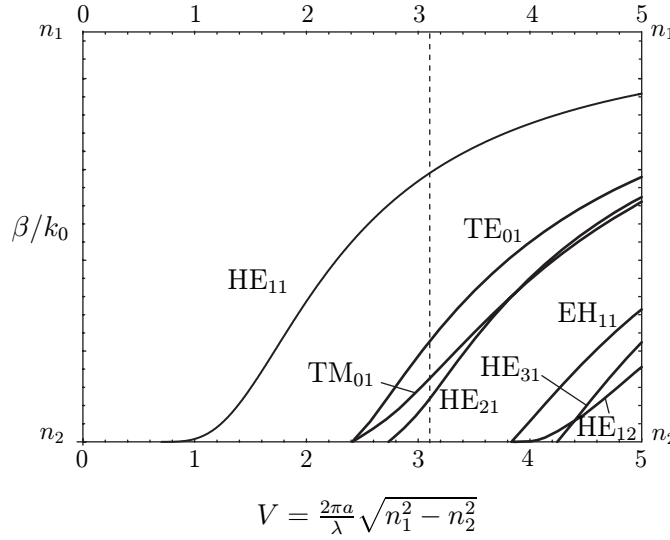
Figure 1. Normalized propagation constant β/k_0 versus V parameter for the first seven modes in the fibre. The dashed vertical line is located at $V = 3.11$ which corresponds to the three trapping configurations considered in this paper.

2.2. The fundamental HE$_{11}$ mode with quasi-linear polarization

The $\vec{E}$ field equations of the fundamental HE$_{11}$ mode with quasi-linear polarization outside the fibre, i.e. for $r > a$, are given by [7]

$$E_x(r, \phi, z, t) = A_{11} \frac{\beta_{11}}{2q_{11}} \frac{J_1(h_{11}a)}{K_1(q_{11}a)} [(1 - s_{11})K_0(q_{11}r) \cos(\varphi_0) \\ + (1 + s_{11})K_2(q_{11}r) \cos(2\phi - \varphi_0)] \exp[i(\omega t - \beta_{11}z)], \tag{1}$$

$$E_y(r, \phi, z, t) = A_{11} \frac{\beta_{11}}{2q_{11}} \frac{J_1(h_{11}a)}{K_1(q_{11}a)} [(1 - s_{11})K_0(q_{11}r) \sin(\varphi_0) \\ + (1 + s_{11})K_2(q_{11}r) \sin(2\phi - \varphi_0)] \exp[i(\omega t - \beta_{11}z)], \tag{2}$$

$$E_z(r, \phi, z, t) = iA_{11} \frac{J_1(h_{11}a)}{K_1(q_{11}a)} K_1(q_{11}r) \cos(\phi - \varphi_0) \exp[i(\omega t - \beta_{11}z)], \tag{3}$$

where

$$s_{11} = \left[\frac{1}{(h_{11}a)^2} + \frac{1}{(q_{11}a)^2} \right] \left[\frac{J_1'(h_{11}a)}{h_{11}aJ_1(h_{11}a)} + \frac{K_1'(q_{11}a)}{q_{11}aK_1(q_{11}a)} \right]^{-1}, \tag{4}$$

$$h_{11} = \sqrt{k_0^2 n_1^2 - \beta_{11}^2}, \tag{5}$$

$$q_{11} = \sqrt{\beta_{11}^2 - k_0^2 n_2^2}. \tag{6}$$

In the equations above, $J(x)$ is the Bessel function of the first kind and $K(x)$ the modified Bessel function of the second kind, $J'(x)$ ($K'(x)$) designates $dJ(x)/dx$ ($dK(x)/dx$), a denotes
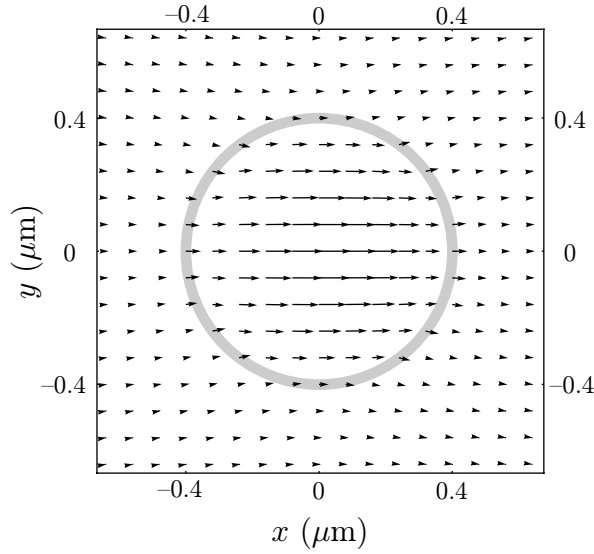
Figure 2. Field plot of the electric field component perpendicular to the fibre axis $\vec{E}_\perp = (E_x, E_y)$ for the HE$_{11}$ mode at $t = 0$, $z = 0$ and for $\varphi_0 = 0$ (see equations (1) and (2)). The fibre is indicated by the grey circle. The following parameters have been used: $a = 400$ nm, $n_1 = 1.452$, $n_2 = 1$, and $\lambda = 850$ nm.

the radius of the fibre, β_{11} the propagation constant of the HE$_{11}$ mode, and the angle φ_0 gives the polarization direction of the transverse electric field $\vec{E}_\perp = (E_x, E_y)$, with $\varphi_0 = 0$ leading to x-polarization and $\varphi_0 = \pi/2$ to y-polarization. A_{11} is a normalization constant of the fields that links the total power to the maximal field amplitude [15]. The quantity q_{11} in equation (6) is particularly relevant since it fixes the scale of the decay length of the fields outside the fibre which can be defined as $\Lambda_{11} = 1/q_{11}$. The HE$_{11}$ is a hybrid mode since it is neither transversal electric (TE) nor transversal magnetic (TM) because the axial-field components E_z and H_z are not zero [14]. The designation of quasi-linear polarization stems from the fact that E_z has a $\pi/2$ dephasing with respect to $\vec{E}_\perp$, which results in elliptical polarization except where $E_z = 0$.

Figure 2 shows a vectorial plot of the electric-field component transverse to the fibre axis $\vec{E}_\perp = (E_x, E_y)$ at $t = 0$ and $z = 0$, with φ_0 set to zero. Note that the equations of the electric field inside the fibre used in this figure are not explicitly given here but can be found in [7]. The surface of the fibre is indicated by a grey circle. The calculations have been performed for a wavelength of $\lambda = 850$ nm. The decay length of the evanescent field for these parameters is $\Lambda_{11} = 164$ nm.

2.3. The TE$_{01}$ mode

We now present the $\vec{E}$ field equations of the TE$_{01}$ mode for $r > a$ [14]. As can be seen from figure 1, the TE$_{01}$ has, like the TM$_{01}$, a cut-off value of $V = 2.405$. This is the lowest cut-off value of any non-fundamental mode and thus sets the single mode condition of a step-index optical fibre.

$$E_\phi(r, \phi, z, t) = -\frac{\omega\mu}{q_{01}} \frac{J_0(h_{01}a)}{K_0(q_{01}a)} B_{01} K_1(q_{01}r) \exp[i(\omega t - \beta_{01}z)],$$
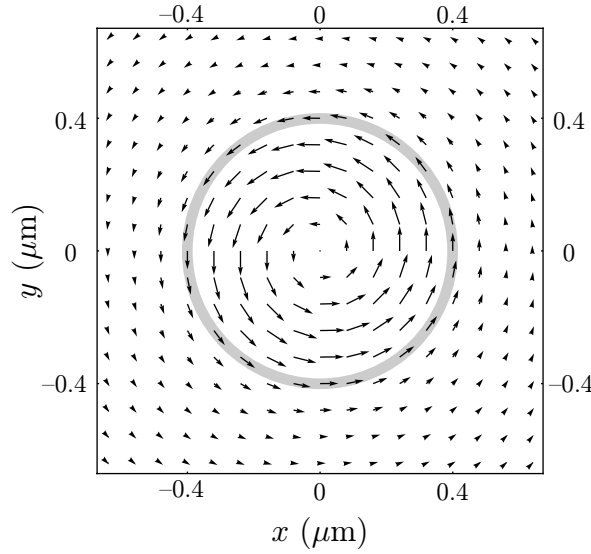
$$E_z(r, \phi, z, t) = E_r(r, \phi, z, t) = 0,$$

(7)

Figure 3. Field plot of the electric field $\vec{E}$ for the TE_{01} mode at $t = 0$ and $z = 0$ (see equation (7)). The fibre is indicated by the grey circle. The fibre parameters are identical to figure 2.

where

$$h_{01} = \sqrt{k_0^2 n_1^2 - \beta_{01}^2}, \tag{8}$$

$$q_{01} = \sqrt{\beta_{01}^2 - k_0^2 n_2^2}, \tag{9}$$

β_{01} denotes the propagation constant of the TE_{01} mode and B_{01} is the normalization constant of the field amplitude. The TE_{01} is classified as a TE mode since it has a vanishing z-component of the electric field. Furthermore, the only non-vanishing electric field component is E_ϕ. The TE_{01} thus possesses only one linearly independent polarization state. The corresponding orthogonal polarization state is the fibre eigenmode TM_{01}. These two modes split due to the distinct influence of the fibre–vacuum boundary on the different $\vec{E}$ polarization directions.

A vectorial plot of the $\vec{E}$ field at $t = 0$ and $z = 0$ is shown in figure 3. The equations of the TE_{01} mode inside the fibre used for this figure can be found in several textbooks, see for example [14, 16]. The calculations have been performed for the same parameters as in figure 2. As shown in figure 3, $\vec{E}$ vanishes at $r = 0$, which, together with the azimuthal symmetry of E_ϕ, produces a toroidal shape of the field amplitude distribution. The decay length of the evanescent field for the given parameters is $\Lambda_{01} = 277$ nm.

2.4. The HE_{21} mode with quasi-linear polarization

The field equations of the HE_{21} mode with quasi-linear polarization for $r > a$ are given by [14]

$$E_x(r, \phi, z, t) = -A_{21} \frac{\beta_{21}}{2q_{21}} \frac{J_2(h_{21}a)}{K_2(q_{21}a)} [(1 - 2s_{21})K_1(q_{21}r)\cos(\phi + 2\phi_0)$$
$$+ (1 + 2s_{21})K_3(q_{21}r)\cos(3\phi + 2\phi_0)]\exp[i(\omega t - \beta_{21}z)], \tag{10}$$
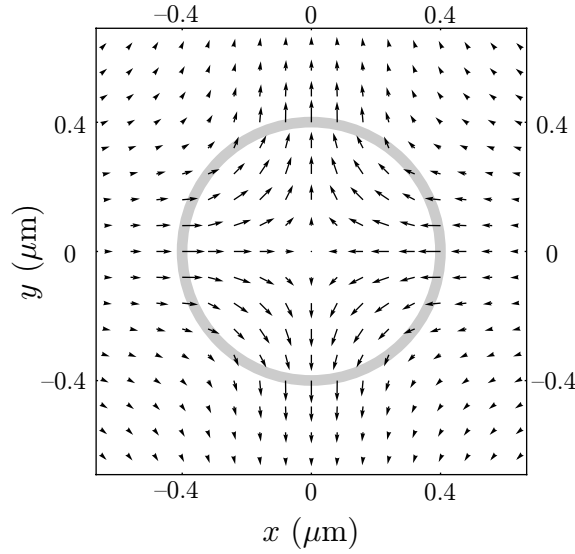
Figure 4. Field plot of the electric field component perpendicular to the fibre axis $\vec{E}_\perp = (E_x, E_y)$ for the HE$_{21}$ mode at $t = 0$, $z = 0$ and for $\phi_0 = 0$ (see equations (10) and (11)). The fibre is indicated by the grey circle. The fibre parameters are identical to figure 2.

$$E_y(r, \phi, z, t) = A_{21} \frac{\beta_{21}}{2q_{21}} \frac{J_2(h_{21}a)}{K_2(q_{21}a)} [(1 - 2s_{21}) K_1(q_{21}r) \sin(\phi + 2\phi_0)$$
$$- (1 + 2s_{21}) K_3(q_{21}r) \sin(3\phi + 2\phi_0)] \exp[i(\omega t - \beta_{21}z)], \tag{11}$$

$$E_z(r, \phi, z, t) = -iA_{21} \frac{J_2(h_{21}a)}{K_2(q_{21}a)} K_2(q_{21}r) \cos(2(\phi + \phi_0)) \exp[i(\omega t - \beta_{21}z)], \tag{12}$$

where

$$s_{21} = \left[\frac{1}{(h_{21}a)^2} + \frac{1}{(q_{21}a)^2} \right] \left[\frac{J_2'(h_{21}a)}{h_{21}a J_2(h_{21}a)} + \frac{K_2'(q_{21}a)}{q_{21}a K_2(q_{21}a)} \right]^{-1}, \tag{13}$$

$$h_{21} = \sqrt{k_0^2 n_1^2 - \beta_{21}^2}, \tag{14}$$

$$q_{21} = \sqrt{\beta_{21}^2 - k_0^2 n_2^2}, \tag{15}$$

β_{21} denotes the propagation constant of the HE$_{21}$ mode and A_{21} is the normalization constant of the field amplitude. ϕ_0 determines the polarization direction of $\vec{E}_\perp$, with $\phi_0 = 0$ and $\phi_0 = \pi/4$ leading to two orthogonal polarization states of the transverse electric field. The HE$_{21}$ is a hybrid mode with six non-vanishing components of the $\vec{E}$ and $\vec{H}$ fields. Like for the HE$_{11}$, the designation of quasi-linear polarization stems from the fact that E_z has a $\pi/2$ dephasing with respect to $\vec{E}_\perp$.

Figure 4 shows a vectorial plot of the electric field component transversal to the fibre axis $\vec{E}_\perp = (E_x, E_y)$ at $t = 0$ and $z = 0$ with ϕ_0 set to zero. Again, the equations of the HE$_{21}$ mode

inside the fibre used for this figure can be found in several textbooks [14, 16]. The calculations have been performed for the same parameters as in figure 2 with a polarization direction given by $\phi_0 = 0$, leading to a decay length of the evanescent field of $\Lambda_{21} = 420$ nm.

3. HE$_{11}$+TE$_{01}$ trap

We now show that an evanescent field surface trap for cold atoms can be obtained from the interference between the fundamental HE$_{11}$ mode, which we assume to be quasi-linearly polarized, and the TE$_{01}$ mode. By choosing the appropriate power distribution between the modes, an array of local minima of the field intensity at any distance from the fibre surface can be created at the positions where the two fields optimally cancel. For blue-detuned light with respect to the atomic transition frequency a dipole force proportional to the negative gradient of the field intensity is then exerted on the atoms [11] confining them in the intensity minima.

As an example, we discuss the properties of the above trap for caesium atoms. The trap can be created with 50 mW of light at a wavelength of 850.5 nm and the same fibre parameters as in section 1. This power is realistic for such a fibre in vacuum: we could experimentally show that appropriately produced fibres with an even smaller radius of 250 nm carry more than 300 mW of power in such conditions without fusing. With 72% of the power propagating in the HE$_{11}$ mode and 28% in the TE$_{01}$ mode, a trap for cold caesium atoms with a trapping minimum at 134 nm from the fibre surface is formed. The depth of the trap is 0.92 mK and the trapping lifetime resulting from heating due to spontaneous scattering of photons exceeds 100 s for caesium atoms with an initial kinetic energy corresponding to 100 μK.

Figure 5 shows a contour plot of the trapping potential including the van der Waals (vdW) surface potential [17] in the plane $z = 4.61 \, \mu$m. We note that the vdW form of the potential is only valid at distances closer than $\lambda_{D2}/10$ from the fibre surface where $\lambda_{D2} = 852.1$ nm is the wavelength of the Cs D2 transition [12]. For larger distances, the Casimir–Polder (CP) form should in general be used. In spite of this fact, we use the vdW potential of an infinite planar silica surface [11] for our calculations because it overestimates the surface interaction at distances larger than $\lambda_{D2}/10$. It thus corresponds to a conservative estimate in this region and is correct at smaller distances. The fibre surface is indicated by a grey circle and the equipotential lines are labelled in millikelvin (mK). The trapping minimum is located at $\phi = \pi/2, r = 534$ nm and $z = 4.61 \, \mu$m. The trapping minimum lies on the y-axis because here the polarization of the two modes matches and the interference is maximally destructive. This polarization matching between the two modes can be understood when comparing figures 2 and 3. Note that while destructive interference takes place at $\phi = \pi/2$, there is constructive interference at $\phi = 3\pi/2$. When varying the φ_0 parameter in equations (1)–(3), the polarization direction of the HE$_{11}$ mode can be turned and thereby the azimuthal position of the trap can be varied because the potential has a $\cos^2(\phi - \varphi_0)$ dependence. Using a harmonic potential approximation, we calculate the azimuthal oscillation frequency to be $\omega_\phi/2\pi \approx 1.07$ MHz. The extension of the trap volume in the azimuthal direction for caesium atoms with a kinetic energy corresponding to 100 μK is 34 nm.

The contour plot of the trapping potential in the plane $x = 0$ is shown in figure 6. The fibre surface is indicated by two vertical grey lines. The interference between the modes creates an array of traps in the axial direction with a periodicity given by the beat length of the two co-propagating modes, $z_0 = 2\pi/(\beta_{11} - \beta_{01}) = 4.61 \, \mu$m. In addition, there is a second array of traps on the opposite side of the fibre with same periodicity which is shifted by $z_0/2$. The

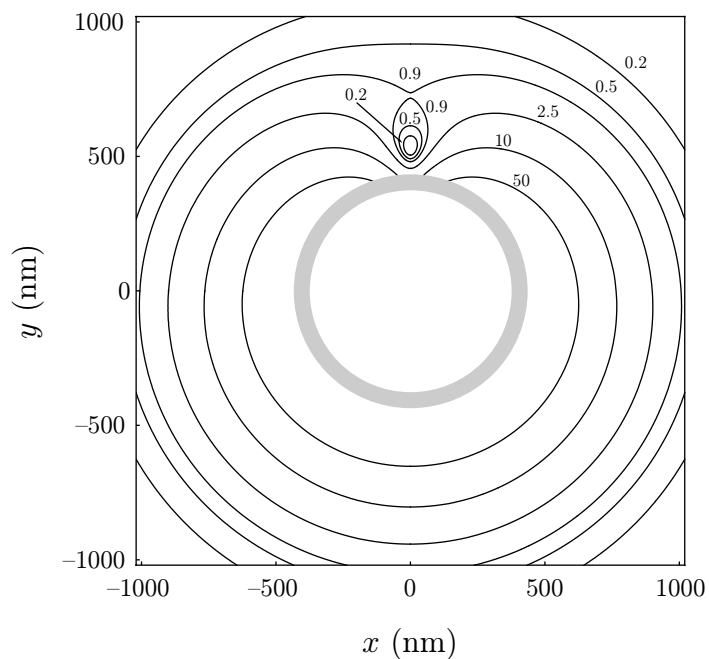**Figure 5.** Contour plot of the $HE_{11} + TE_{01}$ trap in the plane $z = 4.61\,\mu m$ for the following parameters: $P = 50\,mW$, $\tau = 0.72$, $\lambda = 850.5\,nm$, $a = 400\,nm$, $n_1 = 1.452$ and $n_2 = 1$. The fibre surface is indicated by the grey circle and the equipotential lines are labelled in mK.

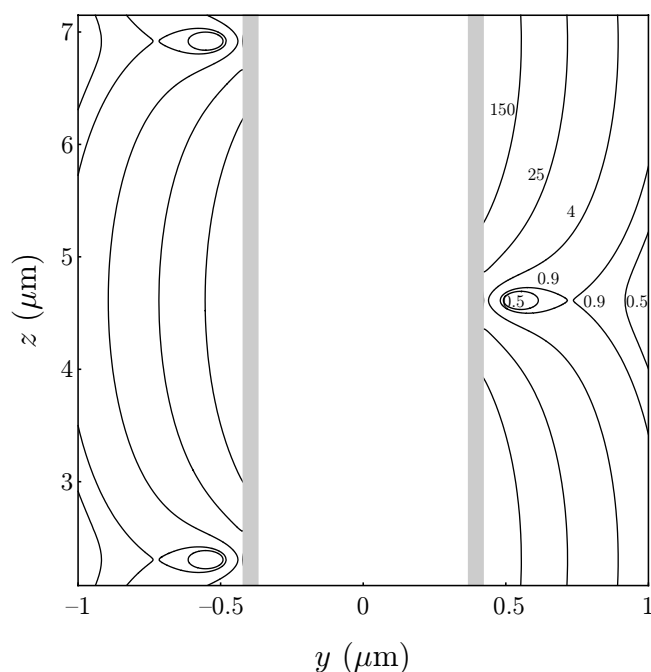**Figure 6.** Contour plot of the $HE_{11} + TE_{01}$ trap in the plane $x = 0$ for the same parameters as in figure 5. The fibre surface is indicated by the two vertical grey lines and the equipotential lines are labelled in mK.
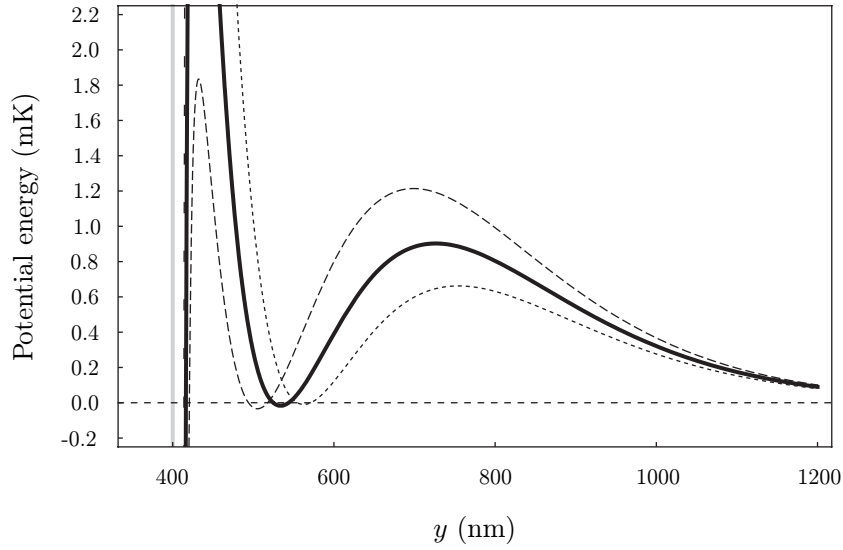
Figure 7. Plot of the trapping potential versus the position along the y-axis for $P_{11} = \tau_0 P$ (solid line), $P_{11} = (\tau_0 + \sigma)P$ (dotted line) and $P_{11} = (\tau_0 - \sigma)P$ (dashed line). The parameters are the same as in figure 5. The fibre surface is indicated by the vertical grey line.

potential has a $\sin^2((\beta_{11} - \beta_{01})z)$ dependence in the axial direction. The axial trapping frequency is calculated to be $\omega_z/2\pi \approx 528\,\text{kHz}$. The extension of the trap volume in this direction for caesium atoms with a kinetic energy corresponding to $100\,\mu\text{K}$ is 68 nm.

Figure 7 shows the trapping potential along the y-axis. The fibre surface is indicated by a vertical grey line. The solid black line corresponds to the sum of the light-induced potential and the vdW potential when 72% of the power propagates in the HE_{11} mode. The dashed and dotted lines correspond to the same potential assuming slightly different power distributions between the modes: we define the parameter τ such that $P_{11} = \tau P$ and $P_{01} = (1 - \tau)P$, where P denotes the total power transmitted through the fibre, P_{11} the power propagating in the HE_{11} mode, and P_{01} the power propagating in the TE_{01} mode. We assume that τ can be controlled with a precision of $\sigma = 0.05\sqrt{\tau_0(1 - \tau_0)}$, i.e. $\sigma = 0.025$ for $\tau_0 = 0.5$. For the case of $\tau_0 = 0.72$, the power distribution between the modes τ would then be controlled within ± 0.022. We consider this value to be a conservative assumption for the precision of the power distribution between the two modes. For the case of $P_{11} = (\tau_0 + \sigma)P$ (dotted line), the trap is 27% shallower compared with the trap for $P_{11} = \tau_0 P$ (solid line), whereas for the case of $P_{11} = (\tau_0 - \sigma)P$ (dashed line), the trap is 30% deeper. While the trap depth increases when decreasing τ, the trapping minimum is also shifted towards the fibre. When further decreasing τ the depth of the trap thus drastically reduces because the vdW potential becomes larger than the light-induced potential. Furthermore, the potential barrier in the direction towards the fibre becomes narrower which would eventually lead to tunnelling of the atoms. The parameters presented here have been chosen in such a way that even with realistic experimental uncertainties the trap remains sufficiently deep and the tunnelling is negligible compared with the trapping lifetime. Note that the total potential is negative at its minimum due to the influence of the vdW potential. Since the z-component of the electric field in the HE_{11} mode vanishes at $\phi = \pi/2$, the polarization in the two modes perfectly matches at the intensity minimum and the vdW potential at this

position is the only influence on the atoms. We calculate the radial trapping frequency to be $\omega_r/2\pi \approx 770\,\text{kHz}$ and the extension of the trapping volume in the radial direction for caesium atoms with a kinetic energy corresponding to $100\,\mu\text{K}$ is $47\,\text{nm}$.

The calculations of the lifetime have been performed assuming caesium atoms with an initial kinetic energy equivalent to $100\,\mu\text{K}$ trapped in a three-dimensional classical harmonic potential with oscillation amplitudes corresponding to the above given extensions of the trapping volume. Note that the trap is not perfectly symmetric along the y-axis (see figure 7), we account for this fact by biasing the oscillation amplitude in this direction. From that, the mean-squared field amplitude at the position of the atom has been calculated by integrating over all possible classical oscillation modes. Using this method, we find a scattering rate of $39\,\text{photons s}^{-1}$ and a trapping lifetime of $108\,\text{s}$.

4. $HE_{11} + HE_{21}$ trap

We now consider the trap arising from the interference between the HE_{11} and the HE_{21} modes. It is created using $25\,\text{mW}$ of light at a wavelength of $849.0\,\text{nm}$ and the same fibre parameters as in section 1. The polarization orientation of the modes has been chosen such that the trap forms at $\phi = 0$. This corresponds to $\varphi_0 = \phi_0 = 0$ in equations (1)–(3) and (10)–(12), respectively. With 84% of the power propagating in the HE_{11} mode, i.e. $\tau = 0.84$ (see section 2), a trap at $152\,\text{nm}$ from the fibre surface is formed. The depth of the trap is $1.2\,\text{mK}$ and the trapping lifetime resulting from spontaneous scattering of photons exceeds $100\,\text{s}$ for caesium atoms with an initial kinetic energy corresponding to $100\,\mu\text{K}$.

Figure 8 shows a contour plot of the trapping potential in the plane $z = 3.45\,\mu\text{m}$. The two dashed lines with their origin at the centre of the trap indicate the two directions with minimal potential barrier which, by consequence, determine the depth of the trap (see figure 11). The trapping minimum is at $\phi = 0$, $r = 552\,\text{nm}$ and $z = 3.45\,\mu\text{m}$. It lies on the x-axis because here the polarization of the two modes matches and the interference is maximally destructive (see figures 2 and 4). However, unlike the $HE_{11} + TE_{01}$ trap considered in section 2, the polarization matching between the two modes is not perfect. This is due to the fact that the ratio $E_z/|\vec{E}_\perp|$ at the trapping minimum is different for the two modes and, therefore, the electric fields never cancel completely. Indeed, this stems from the orientation of $\vec{E}_\perp$ at the position of the trap. When the transverse electric field is perpendicular to the fibre surface, a non-vanishing z-component of the electric field arises [16]. This polarization configuration results in a more intense evanescent field allowing the creation of a trap comparable to the one presented in section 2 with only 50% of the power. As a drawback, the intensity at the trapping minimum is not zero. When varying the parameters φ_0 and ϕ_0 in equations (1)–(3) and (10)–(12), respectively, the polarization direction of the two modes can be rotated and thereby the azimuthal position of the trap can be varied. We calculate the azimuthal oscillation frequency to be $\omega_\phi/2\pi \approx 330\,\text{kHz}$. The extension of the trapping volume in the azimuthal direction is $104\,\text{nm}$.

Figure 9 shows the contour plot of the trapping potential in the plane $y = 0$. The potential has a $\sin^2((\beta_{11} - \beta_{21})z)$ dependence in the axial direction plus the offset due to the unbalanced z-components of the electric fields of the two modes, leading to an axial array of traps with periodicity $z_0 = 2\pi/(\beta_{11} - \beta_{21}) = 3.45\,\mu\text{m}$. Again, there is a second array of traps at the opposite side of the fibre with same periodicity and shifted by $z_0/2$. We calculate the axial trapping frequency and the extension of the trapping potential in the axial direction to be $\omega_z/2\pi \approx 610\,\text{kHz}$ and $58\,\text{nm}$, respectively.
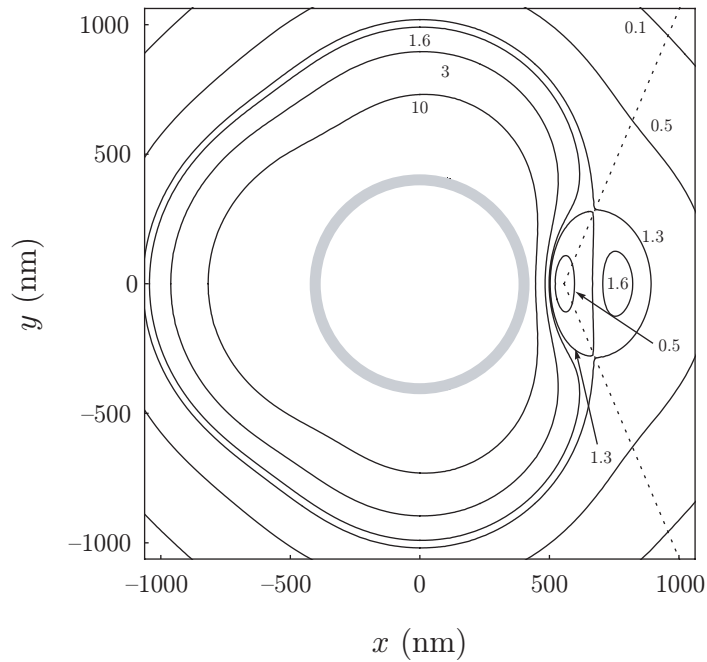
Figure 8. Contour plot of the $HE_{11} + HE_{21}$ trap in the plane $z = 3.45\,\mu m$ for the following parameters: $P = 25\,mW$, $\tau = 0.84$, $\lambda = 849.0\,nm$, $a = 400\,nm$, $n_1 = 1.452$ and $n_2 = 1$. The two directions with minimal potential barrier are indicated by the dashed lines. The fibre surface is indicated by the grey circle and the equipotential lines are labelled in mK.
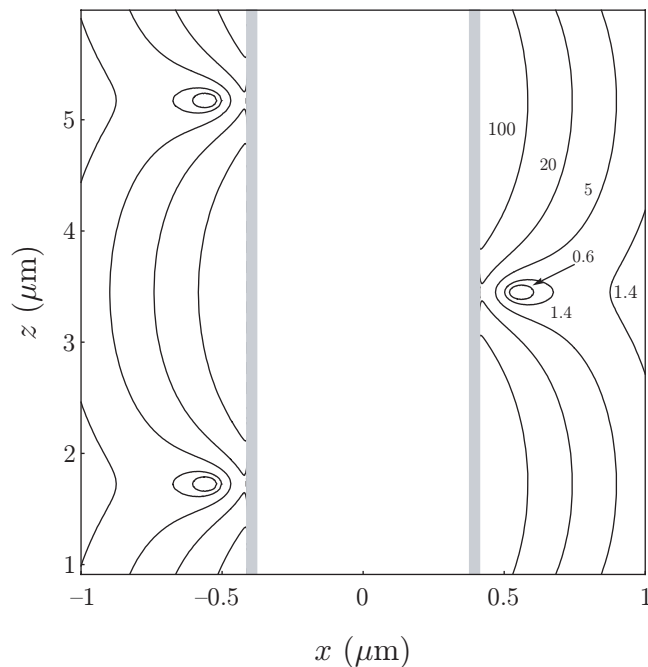

Figure 9. Contour plot of the $HE_{11} + HE_{21}$ trap in the plane $y = 0$ for the same parameters as in figure 8. The fibre surface is indicated by the two vertical grey lines and the equipotential lines are labelled in mK.
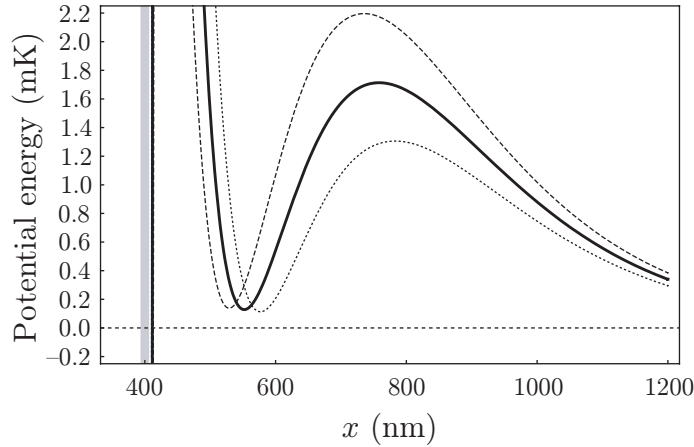
Figure 10. Plot of the trapping potential versus the position along the x-axis for $P_{11} = \tau_0 P$ (solid line), $P_{11} = (\tau_0 + \sigma)P$ (dotted line) and $P_{11} = (\tau_0 - \sigma)P$ (dashed line). The parameters are the same as in figure 8. The fibre surface is indicated by the vertical grey line.
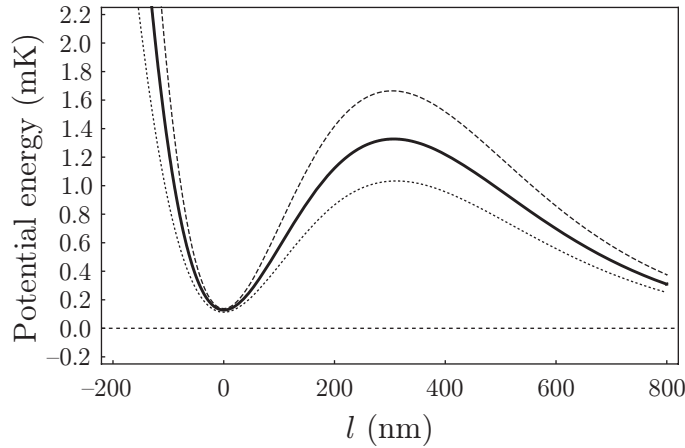

Figure 11. Plot of the trapping potential versus the position along the direction of minimal potential barrier $l(\tau)$ for $P_{11} = \tau_0 P$ (solid line), $P_{11} = (\tau_0 + \sigma)P$ (dotted line) and $P_{11} = (\tau_0 - \sigma)P$ (dashed line). The parameters are the same as in figure 8.

Figure 10 shows the trapping potential versus the position along the x-axis. The solid black line shows the radial trap for $P_{11} = \tau_0 P$, the dashed line for $P_{11} = (\tau_0 - \sigma)P$ and the dotted line for $P_{11} = (\tau_0 + \sigma)P$, with $\tau_0 = 0.84$ and $\sigma = 0.018$. Here, P denotes the total power propagating through the fibre and P_{11} the power propagating in the HE_{11} mode. Again, τ is assumed to be controlled with a precision of $\sigma = 0.05\sqrt{\tau_0(1 - \tau_0)}$. The light-induced potential does not vanish at the minimum due to the mismatching in the polarization between the two modes. This leads to a higher scattering rate of 57 photons s^{-1} compared with the trap presented in section 2. The radial trapping frequency is $\omega_r/2\pi \approx 970\,\text{kHz}$ and the extension of the trapping volume in the radial direction 37 nm. Note that the depth of the potential shown in figure 10 does not correspond to the depth of the trap because, as mentioned above, the direction with minimal potential barrier for the atoms is not radial. Figure 11 therefore shows the trapping potential

against the position along the direction with minimal potential barrier. The solid, dashed and dotted lines have been calculated for the same values of τ as in figure 10. We define the direction with minimal potential barrier l as the straight line that connects the potential minimum in the trap with the lowest local potential maximum. Note that l depends on τ and has, per definition, its origin at the trapping minimum. Hence, the three minima of the potential profiles shown in figure 11 are located at $l = 0$. The trap depth is then found to be 1.2 mK. For the case of $P_{11} = (\tau_0 + \sigma)P$ (dotted line) the trap is 33% shallower compared with the trap for $P_{11} = \tau_0 P$ (solid line), whereas for the case of $P_{11} = (\tau_0 - \sigma)P$ (dashed line) the trap is 17% deeper. Finally, we calculate a trapping lifetime of 106 s. Again, the tunnelling through the potential barrier in the radial direction towards the fibre (see figure 10) is negligible compared with the lifetime of the atoms in the trap.

5. HE$_{21}$ + TE$_{01}$ trap

Finally, we consider the trap arising from the interference between the TE$_{01}$ and the HE$_{21}$ modes. It can be created using 30 mW of light at a wavelength of 851.0 nm and the same fibre parameters as in the above sections. The polarization orientation of the modes has been chosen such that the trap forms at $\phi = 3\pi/4$ and at $\phi = -\pi/4$. Note that this trapping configuration has two trapping minima in the same z-plane, whereas in the traps discussed before there is only one trapping minimum per z-plane. The polarization orientation corresponds to $\phi_0 = 0$ in equations (10)–(12) for the HE$_{21}$ mode. With 68% of the power propagating in the TE$_{01}$ mode, i.e. $\tau = 0.68$ (see section 2), a trap for cold caesium atoms with its trapping minimum at 184 nm from the fibre surface is formed. The depth of the trap is 1.4 mK and, as in the above cases, the trapping lifetime resulting from spontaneous scattering of photons exceeds 100 s for caesium atoms with an initial kinetic energy corresponding to 100 μK.

Figure 12 shows a contour plot of the trap in the plane $z = 13.67\,\mu$m. Here, the trapping minima are shown to be at $\phi = 3\pi/4, r = 584$ nm, $z = 13.67\,\mu$m and at $\phi = -\pi/4, r = 584$ nm, $z = 13.67\,\mu$m because the polarization in the two modes matches at these positions. This is apparent when comparing figures 3 and 4. As for the HE$_{11}$ + TE$_{01}$ case, the polarization matching between the two modes is perfect because the z-component of the electric field in the HE$_{21}$ mode vanishes at the position of the trap. We calculate the azimuthal oscillation frequency to be $\omega_\phi/2\pi \approx 2.60$ MHz. The extension of the trapping volume in the azimuthal direction is 14 nm. This strong confinement in the azimuthal direction stems from the behaviour of the polarization of the electric field in the two modes at the position of the trap. When increasing ϕ, the polarization of the HE$_{21}$ mode rotates clockwise, whereas the polarization of the TE$_{01}$ mode rotates anticlockwise. This produces a fast polarization mismatching between the two fields when displacing the position along the azimuthal direction and thereby a steep increase of the potential.

Figure 13 shows the contour plot of the trap in the zd-plane, where $d = (y - x)/\sqrt{2}$. The interference between the modes creates four axial arrays of traps with a periodicity of $z_0 = 2\pi/(\beta_{01} - \beta_{21}) = 13.67\,\mu$m. The two trapping minima shown in figure 12 show the azimuthal positions of one pair of arrays. The second pair is shifted with respect to the first one by $\phi = \pi/2$ and $z = z_0/2$. We calculate the axial trapping frequency and the extension of the trapping volume in the axial direction to be $\omega_z/2\pi \approx 204$ kHz and 174 nm, respectively. This elongation of the trap compared with the traps presented in sections 2 and 3 stems from the large beat length between the TE$_{01}$ and the HE$_{21}$ modes.
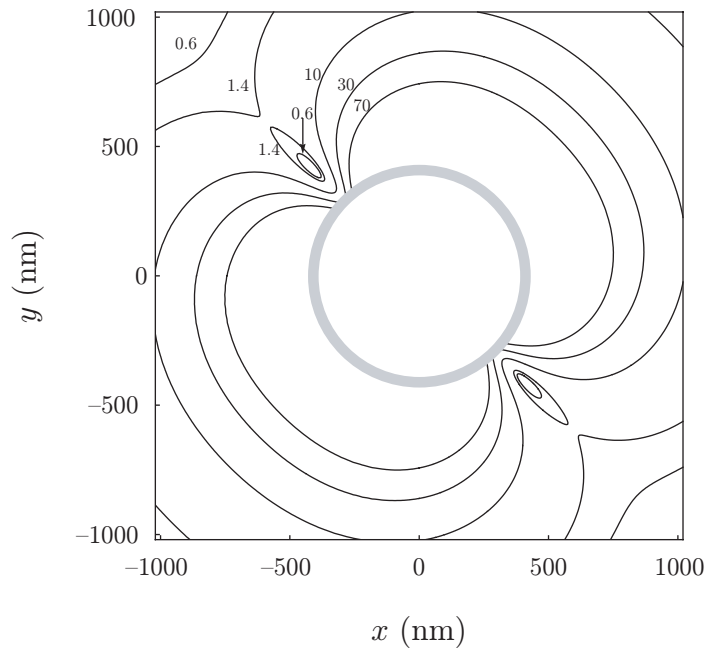
Figure 12. Contour plot of the $TE_{01} + HE_{21}$ trap in the plane $z = 13.67\,\mu\text{m}$ for the following parameters: $P = 30\,\text{mW}$, $\tau = 0.68$, $\lambda = 851.0$ nm, $a = 400$ nm, $n_1 = 1.452$ and $n_2 = 1$. The fibre surface is indicated by the grey circle and the equipotential lines are labelled in mK.
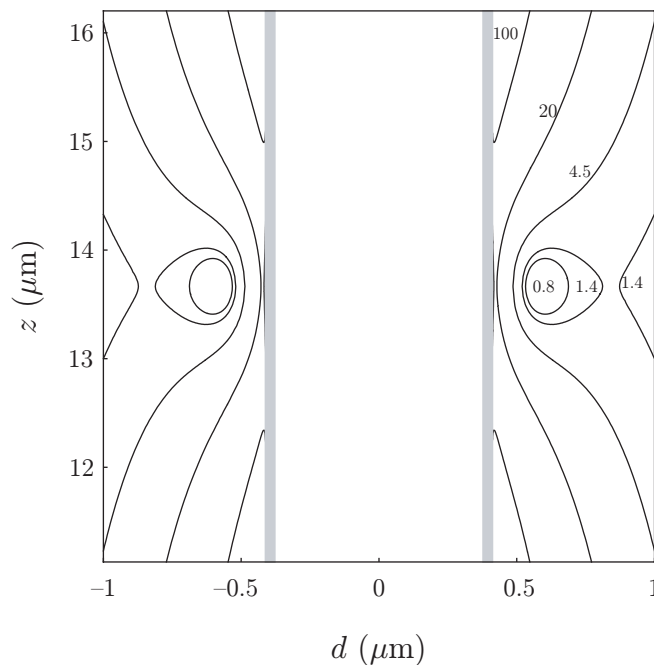

Figure 13. Contour plot of the $TE_{01} + HE_{21}$ trap in the zd-plane, where $d = (y - x)/\sqrt{2}$ for the same parameters as in figure 12. The fibre surface is indicated by the two vertical grey lines and the equipotential lines are labelled in mK.
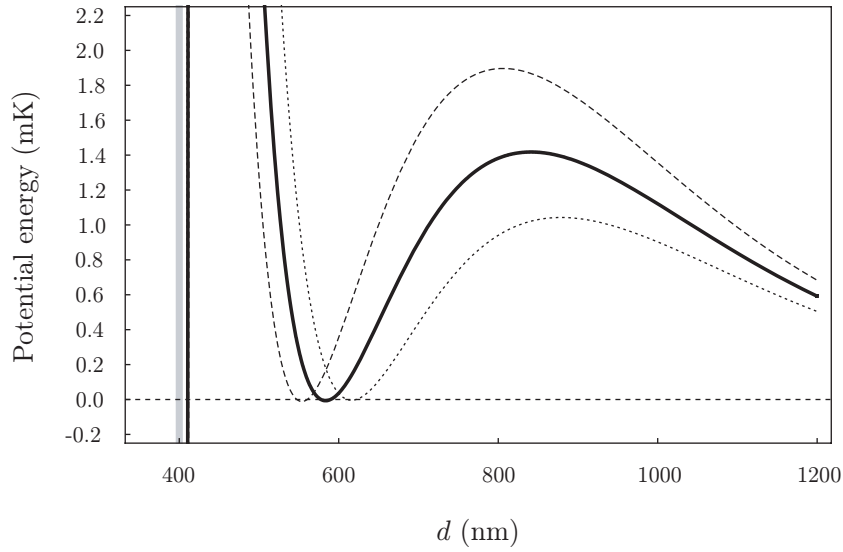
Figure 14. Plot of the trapping potential versus the position along the $d = (y - x)/\sqrt{2}$ axis for $P_{11} = \tau_0 P$ (solid line), $P_{11} = (\tau_0 + \sigma)P$ (dotted line) and $P_{11} = (\tau_0 - \sigma)P$ (dashed line). The parameters are the same as in figure 12. The fibre surface is indicated by the vertical grey line.

Figure 14 shows the radial trapping potential in the above defined zd-plane. The solid black line shows the radial trap for $P_{01} = \tau_0 P$, the dashed line for $P_{01} = (\tau_0 - \sigma)P$, and the dotted line for $P_{01} = (\tau_0 + \sigma)P$, with $\tau_0 = 0.68$ and $\sigma = 0.023$. Again, τ is assumed to be controlled with a precision of $\sigma = 0.05\sqrt{\tau_0(1 - \tau_0)}$. For the case of $P_{11} = (\tau_0 + \sigma)P$, the trap is 25% shallower compared with the trap for $P_{11} = \tau_0 P$, whereas for the case of $P_{11} = (\tau_0 - \sigma)P$, the trap is 36% deeper. Despite the vanishing light-induced potential at the trapping minimum, the total potential does not become significantly negative because the influence of the vdW potential at this distance from the fibre surface is negligible. The radial trapping frequency and the extension of the trapping volume in the radial direction are calculated to be $\omega_r/2\pi \approx 770\,\text{kHz}$ and 47 nm, respectively. Since the beat length between the TE_{01} and the HE_{21} mode is large compared with the beat length in the other two traps, one would expect the radial size of the trap to be large as well. However, the difference in the decay lengths $\Lambda_{21} - \Lambda_{01}$ is not the only factor that influences the radial profile of the trap. It is also determined by the exact functional dependence of the evanescent field for the different modes which results in a similar radial confinement compared with the $HE_{11} + TE_{01}$ and $HE_{11} + HE_{21}$ configurations. Finally, we calculate the scattering rate and the trapping lifetime to be 62 photons s^{-1} and 114 s, respectively.

6. Loading scheme

We have recently demonstrated that a standard magneto-optical trap (MOT) can be normally operated while being overlapped with an ultrathin optical fibre [6]. In order to continuously load the trap from such a MOT the potential barrier separating the trapping minimum from the cold atom reservoir must be eliminated (see, e.g., figure 7). This is possible by adding a red-detuned laser during the loading phase. Starting from the trap presented in section 2 with a τ_0 parameter of 0.89, figure 15 shows the resulting trapping potential as a function of the
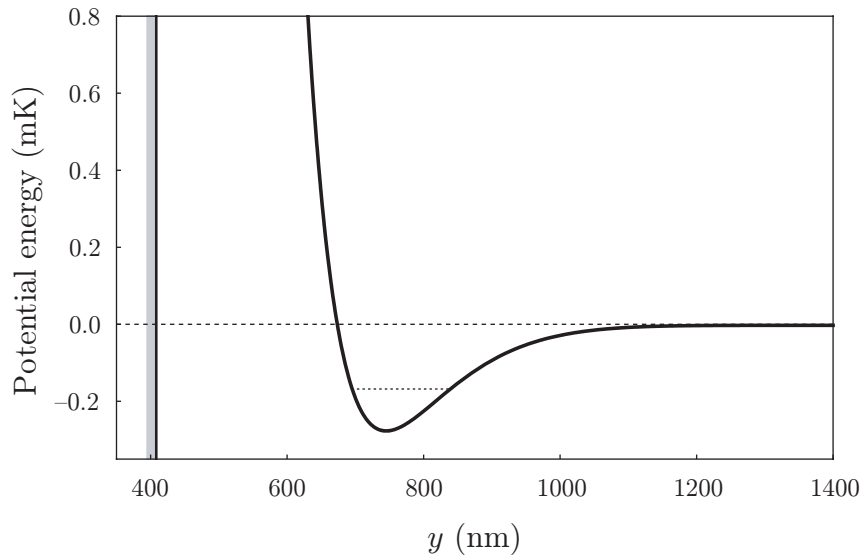
Figure 15. Plot of the trapping potential versus the position along the y-axis for the trap considered in section 2 with $\tau_0 = 0.89$ and 9.2 mW of red-detuned laser light at 970 nm propagating in the TE_{01} mode. The dotted line indicates the mean energy of the atoms transferred from the MOT into the trap. The fibre surface is indicated by the vertical grey line.

radial distance from the fibre for a wavelength of 970 nm and a power of 9.2 mW propagating in the TE_{01} mode. Using the loading rate of the optical micro-trap presented in [18] of up to $100 \, s^{-1}$ and taking into account the smaller trap size and the limited solid angle of capture, we estimate the loading rate of our trap to reach $0.3 \, s^{-1}$, thereby exceeding the one-body loss rate of about $0.1 \, s^{-1}$ due to background gas collisions at a pressure of 10^{-9} Torr [19]. We therefore expect our trap to operate in the collisional blockade regime, yielding a trap occupancy of about 0.5 atoms per site on average [18] corresponding to a total number of 200–300 trapped atoms for a MOT with a $1/\sqrt{e}$-radius of 0.6 mm. By adiabatically switching off the additional red-detuned laser and subsequently restoring the τ parameter, the atoms are then transferred to the purely blue-detuned trap. We note that the resulting ensemble of 200–300 trapped atoms will be optically dense when coupled with a weak resonant probe beam propagating in the fibre.

7. Conclusions

We presented three blue-detuned surface traps for cold atoms based on two-mode interference between the lowest order modes in the evanescent field around a 400 nm radius optical fibre. The trapping potential confines the atoms in all three dimensions. Radially, due to the tailored evanescent field, axially, due to the difference in the phase velocity, and azimuthal, because the different modes have different polarization distributions around the fibre axis. The three traps have a depth of the order of 1 mK and a trapping lifetime that exceeds 100 s for caesium atoms with an initial kinetic energy equivalent to $100 \, \mu K$. Moreover, we have shown that the three traps are robust against experimental uncertainties in the power distribution between the modes. Such an array of optical microtraps in the evanescent field surrounding an optical fibre

IOP Institute of Physics Φ DEUTSCHE PHYSIKALISCHE GESELLSCHAFT

in combination with the highly efficient coupling of the atoms to the fibre modes provides a very promising framework, e.g. for experiments on storing and retrieving light with atomic ensembles. Finally, the selective excitation of the fibre modes is experimentally conceivable. One of the most promising methods is the generation of Gauss–Laguerre modes in free space that match the modes in the fibre [20]. The mapping between the Gauss–Laguerre modes in free space and the modes in an ultrathin optical fibre is therefore currently under investigation in our group.

Acknowledgments

References

[1] Tong L, Gattass R R, Ashcom J B, He S, Lou J, Shen M, Maxwell I and Mazur E 2003 *Nature* **426** 816
[2] Ward J M, O'Shea D G, Shortt B J, Morrissey M J, Deasy K and Nic Chormaic S G 2006 *Rev. Sci. Instrum.* **77** 083105
[3] Nayak K P, Melentiev P N, Morinaga M, Le Kien F, Balykin V I and Hakuta K 2007 *Opt. Express* **15** 5431–8
[4] Warken F, Rauschenbeutel A and Bartholomäus 2008 *Photon. Spectra* **42**(3) 73
[5] Le Kien F, Balykin V I and Hakuta K 2006 *Phys. Rev.* A **73** 013819
[6] Sagué G, Vetsch E, Alt W, Meschede D and Rauschenbeutel A 2007 *Phys. Rev. Lett.* **99** 163602
[7] Le Kien F, Liang J Q, Hakuta K and Balykin V I 2004 *Opt. Commun.* **242** 445
[8] Nayak K P and Hakuta K 2008 *New J. Phys.* **10** 053003
[9] Warken F, Vetsch E, Meschede D, Sokolowski M and Rauschenbeutel A 2007 *Opt. Express* **15** 11952
[10] Dowling J P and Gea-Banacloche J 1996 *Adv. At. Mol. Opt. Phys.* **37** 1
[11] Le Kien F, Balykin V I and Hakuta K 2004 *Phys. Rev.* A **70** 063403
[12] Barnett A H, Smith S P, Olshanii M, Johnson K S, Adams A W and Prentiss M 2000 *Phys. Rev.* A **61** 023608
[13] Christandl K, Lafyatis G P, Lee S-C and Lee J-F 2004 *Phys. Rev.* A **70** 032302
[14] Yariv A 1985 *Optical Electronics* (New York: CBS College)
[15] Bures J and Ghosh R 1999 *J. Opt. Soc. Am.* A **16** 8
[16] Snyder A W and Love J D 2000 *Optical Waveguide Theory* (Boston, MA: Kluwer)
[17] Chevrollier M, Bloch D, Rahmat G and Ducloy M 1991 *Opt. Lett.* **16** 1879
[18] Schlosser N, Reymond G and Grangier P 2002 *Phys. Rev. Lett.* **89** 023005
[19] Metcalf H J and van der Straten P 1999 *Laser Cooling and Trapping* (New York: Springer)
[20] Maurer C, Jesacher A, Fürhapter S, Bernet S and Ritsch-Marte M 2007 *New J. Phys.* **9** 78